Catalysis Science & Technology

ROYAL SOCIETY OF CHEMISTRY

PAPER

View Article Online
View Journal | View Issue

Cite this: *Catal. Sci. Technol.*, 2024, **14**, 1369

Exploring the effect of Brønsted acidity of MFI-type zeolites on catalytic cracking temperature of low density polyethylene†

Soshi Tsubota,[a] Shinya Kokuryo,*[a] Kazuya Tamura,[a] Koji Miyake,*[ab] Yoshiaki Uchida,[a] Atsushi Mizusawa,[c] Tadashi Kubo[c] and Norikazu Nishiyama[ab]

Received 22nd November 2023,
Accepted 13th January 2024

DOI: 10.1039/d3cy01622f

rsc.li/catalysis

Catalytic cracking of plastics using zeolites is a means of promoting the recycling of petrochemical resources. However, the detailed effects of the zeolite Brønsted acidity (acid strength, acid amount, location of acid sites, *etc.*) on the catalytic cracking of plastics have remained unclear. We synthesized MFI-type zeolites with different acid strengths and amounts and compared their low-density polyethylene cracking temperatures with each other. We also aimed to provide guidelines for future catalyst design. Zeolites with controlled acidities were synthesized by introducing different amounts of trivalent metals (Al, Fe, and Ga). The results confirmed that the higher the acid strength and the amount of acid in the zeolites, the lower the cracking temperature of the plastic. However, the cracking temperatures reached a plateau as the amount of acid increased, and the degree of the plateau depended on the acid strength. The acid strength is more important than the acid amount for the cracking temperatures. In addition, we investigated the effect of the location of the acid sites using MFI-type zeolites with different external surface areas and core–shell MFI-type zeolites coated with silicalite-1 as inert shell layers. It was also found that both the acid sites on the outer surface and those within the zeolitic pores were effective in catalytic cracking.

1. Introduction

Over the last few decades, the global production and consumption of plastics have increased at an amazingly high rate. Plastics are extensively used in our surroundings because of their durability and ease of processing. However, their high durability makes plastics an increasing environmental problem. Therefore, immediate and decisive action has been needed to resolve this.[1–4]

The current plastic recycling methods are classified into three categories: material recycling (MR), thermal recycling (TR), and chemical recycling (CR).[5,6] The disadvantages of material recycling and thermal recycling are the degradation of plastics and their environmental impact, respectively. In contrast, chemical recycling is a process in which waste plastics are chemically decomposed and reused as raw materials for fuels and chemical products, and has been attracting attention in recent years as a beneficial recycling process in the chemical industry.[7] The oxygen-free thermal cracking used for chemical recycling essentially emits no carbon dioxide, but it has the disadvantages of high energy consumption due to high-temperature conditions and poor yield of the desired C1–C6+ gases. In contrast, catalytic cracking has been actively studied in recent years because it can lower the decomposition temperature and improve the selectivity of the desired products by using a catalyst such as zeolite or Al-cotaining mesoporous silica.[8–11]

Zeolite is a collective term for porous aluminosilicates, inorganic compounds with a regularly arranged tetrahedral structure (TO_4) centered on metallic elements. Zeolites exhibit shape selectivity owing to their uniform micropores, which leads to improved product selectivity during polymer cracking.[12–15] In addition to these structural properties, zeolites can function as solid acid catalysts. Zeolites are generally composed of tetravalent Si and trivalent Al. The trivalent Al induces a negative charge, and a cation is present near the Al site to balance the total charge. This cation is easily exchangeable, especially when exchanged for H^+, Brønsted acidity is generated.[16,17] On the other hand, various factors contribute to the expression of Lewis acids. One such factor is the aluminum that is exposed outside the zeolite framework. Developing the best catalyst for polymer degradation requires the design of both Lewis and Brønsted acidity.[18–20] A previous study found that an enhancement of

[a] *Division of Chemical Engineering, Graduate School of Engineering Science, Osaka University, 1-3 Machikaneyama, Toyonaka, Osaka 560-8531, Japan.*
E-mail: yasuhiro.shu@cheng.es.osaka-u.ac.jp, kojimiyake@cheng.es.osaka-u.ac.jp
[b] *Innovative Catalysis Science Division, Institute for Open and Transdisciplinary Research Initiatives (ICS-OTRI), Osaka University Suita, Osaka 565-0871, Japan*
[c] *AC Biode Co., Ltd., 498-6 Iwakura Hanazono, Sakyo, Kyoto, 606-0024, Japan*
† Electronic supplementary information (ESI) available. See DOI: https://doi.org/10.1039/d3cy01622f

the Lewis acidity of zeolite leads to a lower LDPE cracking temperature.[21,22] Conversely, the relationship between Brønsted acidity and polymer degradation performance has not yet been clarified. There are many factors related to Brønsted acidity, such as Brønsted acid strength, amount of Brønsted acid, and Brønsted acid sites (external surfaces or internal zeolitic pores).[20,23,24] We expect that verifying the contribution of these factors could provide a clear guideline for catalyst design for polymer cracking, which can help us rationally design catalysts for polymer cracking. It is necessary to prepare zeolites with precisely tuned Brønsted acidities and morphologies to investigate the contribution of Brønsted acidity to polymer cracking.

Previously, we developed various MFI-type zeolites with tuned Brønsted acidities and morphologies. The Brønsted acid strength of zeolite is controlled by substituting Ga and Fe instead of Al.[25–30] The Brønsted acid strength of zeolite depends on the bond length between Al and OH^+, and the shorter the bond length, the stronger the acid strength.[31] The introduction of atoms with a larger atomic radius than Al, such as Fe and Ga, can increase the bond lengths, which generate different Brønsted acid strengths. The amount of Brønsted acid depends on the amount of trivalent atoms.[32] Thus, we changed the amount of the trivalent atoms to control the amount of Brønsted acid sites. Moreover, the location of Brønsted acid sites should be an important factor in the polymer cracking. For example, the accessibility to the external surface of zeolites is quite different from that to the zeolitic micropores. Silicalite-1 coating can control the Brønsted acidity of external surfaces. In this method, MFI-type zeolites with Brønsted acidity can be coated with silicalite-1, which is all silica MFI-type zeolite with no Brønsted acidity. Thus, silicalite-1 coating enables us to investigate the role of Brønsted acidity on the external surfaces.[33–35] In addition, size-controlled MFI-type zeolites can help us investigate the effect of the amount of Brønsted acidity on the external surfaces because the ratio of the external surface area to whole surface area can increase by decreasing the particle size of zeolites.[36–38] In this study, we prepared MFI-type zeolites with precisely controlled Brønsted acidity and morphology based on our previous works and quantitatively elucidated the effect of Brønsted acidity on polymer cracking. In particular, we investigated the cracking temperature of polymer over these zeolites using a thermogravimetric analysis (TGA).

2. Experimental

2.1 Synthesis of MFI zeolites

We synthesized various zeolites referring to our previous works.[39] The precursor solution was prepared using tetraethyl orthosilicate (TEOS) (Wako Pure Chemical Industries Co.), Fe$(NO_3)_3{\cdot}9H_2O$ (Wako Pure Chemical Industries Co.), Al$(NO_3)_3{\cdot}9H_2O$ (Wako Pure Chemical Industries Co.), Ga$(NO_3)_3{\cdot}8H_2O$ (Wako Pure Chemical Industries Co.), 20–25 wt% tetrapropylammonium hydroxide (TPAOH) (Tokyo Chemical Industry Co., Ltd.) and deionized water. The molar ratio of the solution was 85.3 H_2O : 0.25 TPAOH : 1 TEOS. The metal source T was added to the solution such that Si/T = 50, 80, 100, 200, and 300, where T is Fe, Al, or Ga. The precursor solution was then stirred at room temperature for 24 h. The solution was then transferred to an autoclave and crystallized under steam at 453 K for 24 h. The resulting powder was mixed with deionized water and separated by centrifugation. The washing process was repeated several times, followed by drying at 363 K. The as-made sample was calcined at 823 K for 5 h to remove the structure directing agent (SDA). Silicalite-1 was prepared by the same procedure, using only TEOS, TPAOH, and deionized water.

Furthermore, we decreased the amount of deionized water in the precursor solution to control the particle size of the Al-MFI zeolites. For the synthesis of size-controlled MFI zeolites, we used 10 wt% TPAOH (Wako Pure Chemical Industries Co.) instead of 20–25 wt% TPAOH. In particular, we used the precursor solution with a molar ratio of 24.1 or 54.7 H_2O : 0.25 TPAOH : 1 TEOS by fixing Si/Al = 80. The samples were labeled as "Al-80-low" and "Al-80-medium", respectively. We also prepared MFI zeolite by dry gel conversion using the precursor solution with a molar ratio of 85.3 H_2O : 0.25 TPAOH : 1 TEOS by fixing Si/Al = 80 referring to our previous work.[39] The sample was labeled as "Al-80-DGC". Similarly, 10 wt% TPAOH was used for DGC synthesis. In addition, silicalite-1 coating was performed for T-MFI using fumed silica, 10 wt% TPAOH, ethanol (Wako Pure Chemical Industries Co.) and deionized water referring to our previous work.[33]

2.2 Characterization

The crystal structures of the samples were confirmed by X-ray diffraction (XRD) using Cu Kα radiation on a PANalytical X'Pert PRO MPD diffractometer. An energy-dispersive X-ray (EDX) analysis was performed to evaluate the chemical composition using a JCM-7000 microscope (JEOL). To investigate the state of the Fe, Al and Ga species, UV-vis diffuse reflectance spectra were measured with a UV-vis spectrophotometer (Jasco V-570). To observe the crystal size of the samples, scanning electron microscopy (SEM) images were recorded using a JCM-7000 microscope (JEOL). The acidic properties of Fe, Al or Ga-MFI were evaluated by NH_3 temperature programmed desorption (NH_3-TPD) measurements using a BEL CAT II and BEL mass (MicrotracBel). The NH_3-TPD measurement can be used to measure the heat of adsorption of ammonia, which is an indication of the acid strength, in addition to the acid amount of the catalyst.[40] The acid strength was quantified using the following equation:

$$\ln T_p - \ln\left(\frac{A_0 W}{F}\right) = \frac{\Delta H}{R T_p} + \text{const.}$$

where A_0 is the acid amount (mol kg^{-1}), W is the sample weight (kg), T_p is the desorption temperature (K), F is the flow rate of carrier gas (m^3 s^{-1}) and R is the gas constant (J (K^{-1} mol)). ΔH is

the heat of adsorption of ammonia (J mol^{-1}), which is equivalent to the acid strength of the zeolite. The acidic state in the sample was also evaluated using Fourier transform infrared spectroscopy (FT-IR) with acetonitrile (CD_3CN) as the probe molecule.

2.3 LDPE cracking

The catalytic activity of the prepared catalysts was evaluated by cracking of low-density polyethylene (LDPE) using thermogravimetric analysis (TGA).[21] The catalyst/LDPE mixture or pure LDPE was placed in an alumina pan for TGA. The mass ratio of the catalyst/LDPE mixtures was fixed at 20/80. When LDPE is cracked at elevated temperatures, it gasifies and its mass gradually decreases. In this study, "T_{half}" is defined as the temperature at which the mass of LDPE is reduced by half, and we used it as an index for the catalytic activity on LDPE cracking.

3. Results & discussion

Fig. S1† shows that the MFI structure is present in all samples; the absence of peaks originating from the metal oxides of Fe, Al, and Ga indicates that each metal is incorporated into the framework. Fig. S2† shows that there is no significant difference in the particle size or shape when changing the metal source or Si/T ratio, and the same particle structure is confirmed from Fig. S2.† When the Si/T ratio was larger than that listed in Table S1,† there was a difference between the amount of preparation and the measurement results. The measured values were smaller than the Si/T ratio in the preparation, confirming that not all Si atoms were introduced into the framework compared with Fe, Al, and Ga. The above characterization confirmed that Al, Fe, and Ga were introduced into the zeolite framework. The UV bands around 211 and 245 nm are characteristic for Fe^{3+} at isolated tetrahedral framework sites[41] and the UV spectra of Fe-*x* broadened at 250–450 nm as the amount of Fe introduced increased.(Fig. S3†) This fact suggests that excess Fe^{3+} formed Fe_2O_3 in the bulk.[41] In Fig. S4,† the Brønsted acid-derived peak was observed around 2274 cm^{-1} for all samples, whereas for Fe-80, a slight Lewis acid-derived peak was observed around 2306 cm^{-1}.[42,43] This is thought to originate from the Fe_2O_3 formed in the bulk, which is consistent with the UV-vis results.

The NH_3-TPD measurement allows us to measure the heat of adsorption of ammonia, which is an indication of acid strength, in addition to the acid amount of the catalyst. For the three catalysts with similar Si/T ratios, Al-80, Fe-80, and Ga-80, the sample weights were varied (2.5×10^{-4}, 5.0×10^{-4}, 1.0×10^{-3}, 2.0×10^{-3} kg), and the results were plotted using the above method, as shown in Fig. 1. From the slope, the heat of ammonia adsorption for each catalyst was 1.92×10^2 kJ mol^{-1} for Al, 1.55×10^2 kJ mol^{-1} for Ga, and 1.43×10^2 kJ mol^{-1} for Fe.

The TGA curves of LDPE catalytic cracking with silicalite-1 and thermal cracking are shown in Fig. 2. Both only LDPE and LDPE mixed with zeolite gradually gasify, and those masses lose with increasing temperature. Both TGA curves were similar, indicating that silicalite-1 did not work as a catalyst. The T_{half} of silicalite-1/LDPE is approximately 460 °C, as shown in Fig. 2. The cracking temperature when the remaining weight of LDPE is reduced to half is defined as T_{half}.

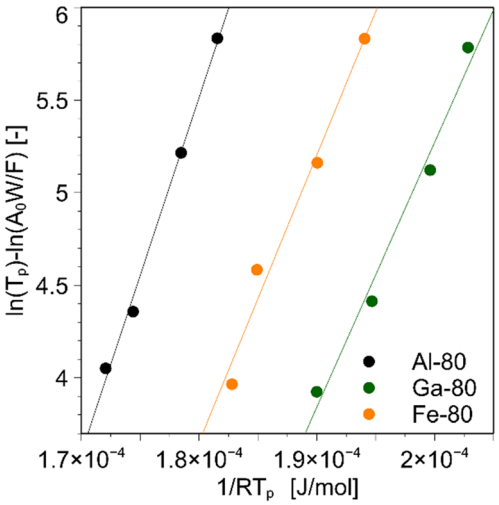

Fig. 1 Quantification of Brønsted acid strength of MFI zeolites.

The smaller the Si/T ratio (*i.e.*, the higher the amount of solid acid), the lower the T_{half} value (Fig. 3). Regardless of the type of metal introduced, the cracking temperature remained constant at about 460 °C in the range of Si/T ratios greater than about 100 with less than a certain amount of acid. This is consistent with the LDPE cracking temperature of silicalite-1 which is an MFI zeolite without a Brønsted acid. It was also observed that the higher the acid strength of the catalyst, the lower the T_{half} value.

The Si/T ratio obtained by EDX analysis is not an accurate amount of acid because it includes the amount of metal that has not been introduced into the catalyst framework.

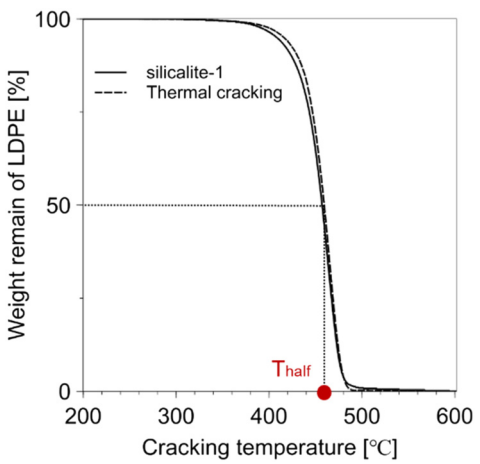

Fig. 2 TGA curve of LDPE cracking using silicalite-1 and without.

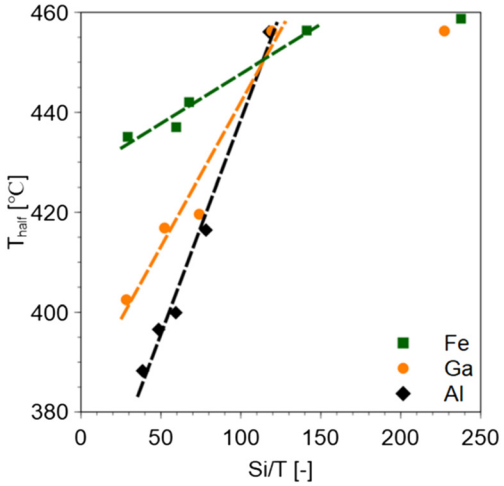

Fig. 3 Relationship between Si and T ratios and T_{half} value of heterometallic MFI zeolite.

Therefore, the amount of ammonia adsorbed by NH_3-TPD was taken as the acid amount of the catalyst, and the relationship between the amount of acid and catalyst cracking temperature was investigated. In the catalytic cracking of LDPE using any zeolite, a decrease in T_{half} was observed as the amount of acid was increased. However, as the acid amount further increased, the cracking temperature plateaued. Fig. 4 suggests that the saturated cracking temperature depends on the acid strength of the zeolite. Therefore, the acid strength has a stronger influence on the catalytic cracking of plastics than the amount of acid.

Similar catalytic cracking of LDPE was performed using MFI-type zeolites with different external surface areas. The TEM images confirmed that different particle sizes were obtained, as shown in Fig. S5.† The specific particle sizes are Al-80-DGC: 30–50 nm, Al-80-low: 200–300 nm, and Al-80-medium: approximately 400 nm, respectively. The particle size of the zeolite was reduced *via* synthesis using the DGC method. This is thought to be due to the higher nucleation density in the early stages of synthesis and the longer time required for crystal growth.[39] Their external surface areas were calculated by the t-method using their N_2 adsorption isotherms. Different external surface areas were obtained and are listed in Table S2.† In addition, similar Si/Al ratios and acid amounts were obtained. Thus, the comparison should be effective in investigating the effects of the external surface areas. Fig. 5 confirms that the larger the outer surface area, the lower the T_{half}. Therefore, the accessibility of plastic molecules into the zeolite pores is very important for catalytic cracking.

Similar catalytic cracking was performed using core–shell zeolites; Al-MFI, Ga-MFI, and Fe-MFI coated by silicalite-1 without Brønsted acid in that outer shell. First, SEM observations were performed to confirm that the silicalite-1 layers were grown epitaxially. Fig. S6† shows that coffin-shaped zeolites were obtained and crystal growth occurred along the *c*-axis after silicalite-1 coating. For Al-MFI, the particle diameters of the sample before core–shell were 0.576 μm to *a* axis and 0.969 μm to *c* axis, whereas they increased to 0.670 μm to *a* axis and 1.28 μm to *c* axis due to silicalite-1 coating. The same increase in particle size was confirmed for Ga-MFI and Fe-MFI by silicalite-1 coating. In addition, Si/T ratios increased after silicalite-1 coating (Table S3†) due to the mass gain of the silicate layer. These results were in accordance with those of our previous study.[33] Therefore, core–shell zeolites were obtained. We plotted the T_{half} values of the core–shell zeolites against the acid amount, as shown in Fig. 6. The cracking temperatures were higher than those obtained with the uncoated zeolite. This indicates that the acid sites on the external surface of the zeolite have a significant effect on the catalytic cracking of LDPE. Meanwhile, the T_{half} values of the core–shell zeolites were lower than that of silicalite-1, indicating that Brønsted acid sites inside the zeolite crystals also contributed to lowering the catalytic cracking temperature of LDPE. From the above, it was

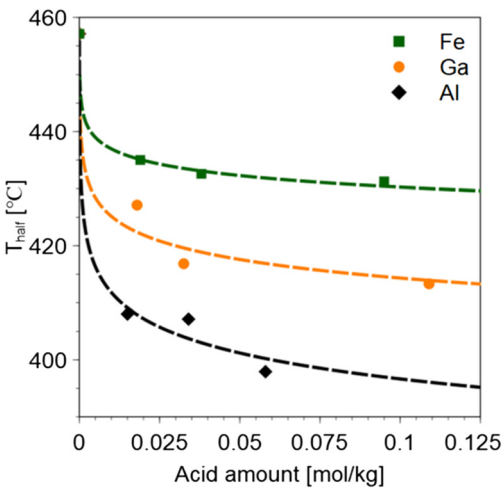

Fig. 4 Relationship between the amount of acid in zeolite and T_{half} value. T_{half} value at 0 mol kg^{-1} represents the data for silicalite-1.

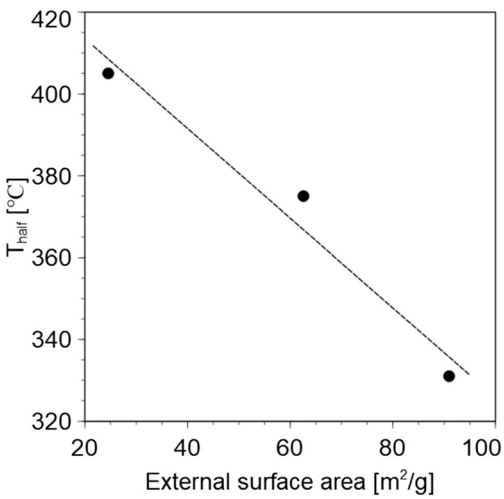

Fig. 5 Relationship between the external surface area of zeolite and T_{half} value.

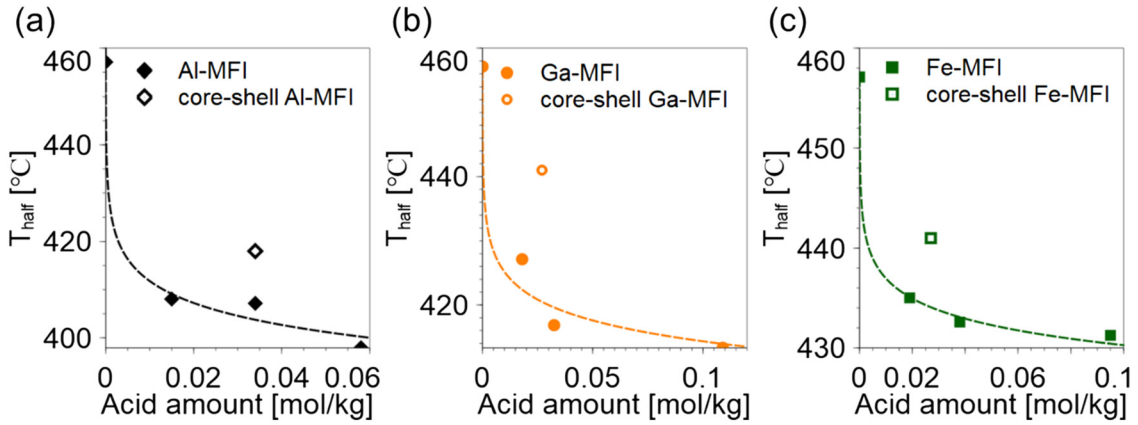

Fig. 6 Comparison of T_{half} between uncoated and core–shell zeolites: (a) Al, (b) Ga, and (c) Fe. T_{half} value at 0 mol kg^{-1} represents the data for silicalite-1.

found that the catalytic cracking of plastics using zeolites takes place in the following two steps. (1) The polymer is cracked at the acid sites on the external surface until it is small enough to enter the zeolite pore. (2) The polymer decomposed in step (1) is further decomposed at the acid point inside the pore to obtain C1–C6+ gas.

Conclusions

In this study, the influence of zeolite acidity on catalytic cracking temperature was investigated to provide clear guidelines for the design of zeolite catalysts for the catalytic cracking of plastics. MFI-type zeolites with controlled acid strength and acid amount were synthesized, and the LDPE cracking temperatures using the MFI-type zeolites were compared. The cracking temperature decreased as the acid amount of the catalyst increased but reached a plateau as the acid amount was further increased. The saturated cracking temperature depends on the acid strength of the zeolites, and it can be said that the acid strength has a stronger influence on catalytic cracking than the acid amount. The LDPE cracking temperature is strongly dependent on the external surface area. Therefore, it is suggested that the accessibility of LDPE molecules into zeolite pores is important. We investigated the LDPE cracking temperature with a core–shell type zeolite with silicalite-1, which has no Brønsted acid sites at the shell layer. The results showed that the LDPE cracking temperature with the core–shell type zeolite was lower than the catalytic cracking temperature with silicalite-1 and higher than that with the uncoated catalyst. These results indicate that not only the acid sites inside the zeolite, but also those on the external surface contribute to the lower LDPE cracking temperature.

Author contributions

Soshi Tsubota: conceptualization, investigation, visualization, writing – original draft. Shinya Kokuryo: conceptualization, investigation, visualization, methodology, writing – review & editing. Kazuya Tamura: methodology, writing – review & editing. Koji Miyake: conceptualization, supervision, visualization, methodology, writing – review & editing. Yoshiaki Uchida: writing – review & editing. Atsushi Mizusawa: methodology, writing – review & editing. Tadashi Kubo: funding acquisition, writing – review & editing. Norikazu Nishiyama: funding acquisition, supervision, resources, writing – review & editing.

Conflicts of interest

There are no conflicts to declare.

Acknowledgements

A part of the present experiments was carried out by using a facility in the Research Center for Ultra-High Voltage Electron Microscopy, Osaka University.

Notes and references

1 E. J. North and R. U. Halden, *Rev. Environ. Health*, 2013, **28**, 1–8.
2 M. F. Ali, S. Ahmed and M. S. Qureshi, *Fuel Process. Technol.*, 2011, **92**, 1109–1120.
3 C. M. Rochman, M. A. Browne, B. S. Halpern, B. T. Hentschel, E. Hoh, H. K. Karapanagioti, L. M. Rios-Mendoza, H. Takada, S. Teh and R. C. Thompson, *Nature*, 2013, **494**, 169–171.
4 R. Geyer, J. R. Jambeck and K. L. Law, *Sci. Adv.*, 2017, **3**, e1700782.
5 J. Hopewell, R. Dvorak and E. Kosior, *Philos. Trans. R. Soc., B*, 2009, **364**, 2115–2126.
6 A. Rahimi and J. M. García, *Nat. Rev. Chem.*, 2017, **1**, 0046.
7 N. Miskolczi, L. Bartha, G. Deák and B. Jóver, *Polym. Degrad. Stab.*, 2004, **86**, 357–366.
8 T. Thiounn and R. C. Smith, *J. Polym. Sci.*, 2020, **58**, 1347–1364.
9 M. Solis and S. Silveira, *Waste Manage.*, 2020, **105**, 128–138.
10 J. Aguado, D. P. Serrano, J. M. Escola and A. Peral, *J. Anal. Appl. Pyrolysis*, 2009, **85**, 352–358.

11 Z. Zhang, K. Gora-Marek, J. S. Watson, J. Tian, M. R. Ryder, K. A. Tarach, L. López-Pérez, J. Martínez-Triguero and I. Melián-Cabrera, *Nat. Sustain.*, 2019, **2**, 39–42.
12 *Zeolites and catalysis: synthesis, reactions and applications*, ed. J. Čejka, A. Corma and S. Zones, Wiley-VCH, Weinheim, 2010.
13 A. Dyer, *An introduction to zeolite molecular sieves*, J. Wiley, Chichester, New York, 1988.
14 J. Kärger, D. M. Ruthven and D. N. Theodorou, *Diffusion in Nanoporous Materials*, Wiley, 1st edn, 2012.
15 J. E. Naber, K. P. De Jong, W. H. J. Stork, H. P. C. E. Kuipers and M. F. M. Post, in *Studies in Surface Science and Catalysis*, Elsevier, 1994, vol. 84, pp. 2197–2219.
16 A. Corma, *Curr. Opin. Solid State Mater. Sci.*, 1997, **2**, 63–75.
17 J. F. Haw, *Phys. Chem. Chem. Phys.*, 2002, **4**, 5431–5441.
18 Z. Wang, L. Wang, Y. Jiang, M. Hunger and J. Huang, *ACS Catal.*, 2014, **4**, 1144–1147.
19 F. Yi, Y. Chen, Z. Tao, C. Hu, X. Yi, A. Zheng, X. Wen, Y. Yun, Y. Yang and Y. Li, *J. Catal.*, 2019, **380**, 204–214.
20 N. Katada, K. Suzuki, T. Noda, G. Sastre and M. Niwa, *J. Phys. Chem. C*, 2009, **113**, 19208–19217.
21 S. Kokuryo, K. Miyake, Y. Uchida, A. Mizusawa, T. Kubo and N. Nishiyama, *Mater. Today Sustain.*, 2022, **17**, 100098.
22 S. Kokuryo, K. Tamura, K. Miyake, Y. Uchida, A. Mizusawa, T. Kubo and N. Nishiyama, *Catal. Sci. Technol.*, 2022, **12**, 4138–4144.
23 Y. Chai, W. Dai, G. Wu, N. Guan and L. Li, *Acc. Chem. Res.*, 2021, **54**, 2894–2904.
24 J. Huang, N. van Vegten, Y. Jiang, M. Hunger and A. Baiker, *Angew. Chem.*, 2010, **122**, 7942–7947.
25 M. Miyamoto, K. Mabuchi, J. Kamada, Y. Hirota, Y. Oumi, N. Nishiyama and S. Uemiya, *J. Porous Mater.*, 2015, **22**, 769–778.
26 V. R. Choudhary, A. K. Kinage and T. V. Choudhary, *Appl. Catal., A*, 1997, **162**, 239–248.
27 C. R. Bayense, A. J. H. P. Van Der Pol and J. H. C. Van Hooff, *Appl. Catal.*, 1991, **72**, 81–98.
28 T. Taniguchi, Y. Nakasaka, K. Yoneta, T. Tago and T. Masuda, *Microporous Mesoporous Mater.*, 2016, **224**, 68–74.
29 J. Perezramirez, *J. Catal.*, 2004, **223**, 13–27.
30 J. Perezramirez, J. Groen, A. Bruckner, M. Kumar, U. Bentrup, M. Debbagh and L. Villaescusa, *J. Catal.*, 2005, **232**, 318–334.
31 A. J. Jones, R. T. Carr, S. I. Zones and E. Iglesia, *J. Catal.*, 2014, **312**, 58–68.
32 W. Mortier, *J. Catal.*, 1978, **55**, 138–145.
33 K. Miyake, R. Inoue, T. Miura, M. Nakai, H. Al-Jabri, Y. Hirota, Y. Uchida, S. Tanaka, M. Miyamoto, S. Inagaki, Y. Kubota, C. Y. Kong and N. Nishiyama, *Microporous Mesoporous Mater.*, 2019, **288**, 109523.
34 K. Miyake and N. Nishiyama, in *Core-Shell and Yolk-Shell Nanocatalysts*, ed. H. Yamashita and H. Li, Springer Singapore, Singapore, 2021, pp. 181–186.
35 K. Miyake, Y. Hirota, K. Ono, Y. Uchida, S. Tanaka and N. Nishiyama, *J. Catal.*, 2016, **342**, 63–66.
36 P. R. H. P. Rao and M. Matsukata, *Chem. Commun.*, 1996, 1441.
37 P. R. Hari Prasad Rao, K. Ueyama and M. Matsukata, *Appl. Catal., A*, 1998, **166**, 97–103.
38 R. Cai, Y. Liu, S. Gu and Y. Yan, *J. Am. Chem. Soc.*, 2010, **132**, 12776–12777.
39 K. Miyake, Y. Hirota, K. Ono, Y. Uchida, M. Miyamoto and N. Nishiyama, *New J. Chem.*, 2017, **41**, 2235–2240.
40 M. Niwa and N. Katada, *Chem. Rec.*, 2013, **13**, 432–455.
41 E. Hensen, Q. Zhu, R. Janssen, P. Magusin, P. Kooyman and R. Vansanten, *J. Catal.*, 2005, **233**, 123–135.
42 C. Pazé, A. Zecchina, S. Spera, G. Spano and F. Rivetti, *Phys. Chem. Chem. Phys.*, 2000, **2**, 5756–5760.
43 J. Jänchen, G. Vorbeck, H. Stach, B. Parlitz and J. H. C. Van Hooff, in *Studies in Surface Science and Catalysis*, Elsevier, 1995, vol. 94, pp. 108–115.